Difference-quotient turbulence model: Analytical solutions for the core region of plane Poiseuille flow

Peter W. Egolf[1] and Daniel A. Weiss[2,*]
[1]*Swiss Federal Laboratories for Materials Testing and Research, CH-8600 Dübendorf, Switzerland*
[2]*Labooratoire PMMH, ESPCI, F-75231 Paris Cedex 05, France*
(Received 25 March 1999; revised manuscript received 7 March 2000)

The difference-quotient turbulence model and an explanation in terms of fluid dynamics is presented. With this model an analytical theory for the symmetric core region of turbulent plane Poiseuille flow is derived. The equations and the solutions reveal an order/disorder transition with analogies in other scientific fields where statistical physics applies. At moderate Reynolds numbers the time-averaged profile of the downstream mean velocity and a second-order fluctuation correlation are described in terms of Bessel functions of the first type. At the infinite Reynolds number limit these solutions converge toward functions which can be described by simple geometric figures. Experimental data confirm the model results.

PACS number(s): 47.27.Eq, 47.27.Gs, 47.27.Jv, 47.60.+i

I. INTRODUCTION

Nowadays theoretical research work on turbulent Poiseuille flow, or channel flow, is mostly the subject of direct numerical simulations, performed for example in 1990 by Gilbert and Kleiser [1] and in 1993 by Sandham [2]. Such calculations yield valuable results, permitting the study of physical behavior of a large number of different phenomena occurring in turbulent flows, e.g., vortex stretching, vortex folding, the occurrence of ejections, sweeps, bursts, etc. Furthermore, direct numerical simulation results more frequently yield a welcome additional contribution to experimental data. Via direct numerical simulations, it is possible to calculate turbulent flows up to a Taylor-Reynolds number of approximately $\mathrm{Re}_\lambda = 200$ [3]. This flow-internal Reynolds number is calculated with a fluctuation velocity and a correlation length and is a measure of the forcing of the fluid-dynamic system. The Taylor-Reynolds number has the advantage of being independent of the way the turbulence is created. This is crucial for the investigation of universal behavior. Experiments have been performed with Reynolds numbers up to $\mathrm{Re}_\lambda = 13\,000$ (e.g., see Ref. [4]).

For fully developed turbulent flows, the extremely large number of degrees of freedom requires computer power not yet available. Therefore, it is still necessary to base calculations on turbulence models which yield a closure of the mathematical problem solving the Navier-Stokes equations [5]. The validity of such models can be qualitatively understood by scaling arguments and therefore the study of their features is relevant from a theoretical point of view as well. With higher-order moment turbulence models it is usually not possible to derive analytical results. Therefore, for our purposes only one-equation models are considered. By simplified considerations it is possible to classify turbulence models into three groups. Crude models only correspond to *identical eddies of equal size*, which only approximately describe the turbulent momentum transport in fluid domains. The most successful approach of this kind was Prandtl's mixing-length theory [6]. When it was first applied to calculate quasistationary turbulent-free-shear-flow problems, it soon became obvious that the mixing length had to be taken as a function of space. Therefore, in a simple way, vortices with continuously varying sizes as a function of space were introduced. But still, only one size type was related to a single space location. Several recently published more sophisticated models are still based on this insufficient conception. A new generation of turbulence models defines—at each space point of turbulent domains—eddies corresponding to *an infinitely large amount of length scales* (e.g., see Ref. [7]).

The difference-quotient turbulence model (DQTM) [8] is an approach containing the essential feature of an infinite number of scales. This model analytically describes fully turbulent-free-shear flows, e.g., turbulent flows behind wakes and jets without empirical constants (see Refs. [9] and [10]). The correlation between theory and experimental data is in each case very convincing. The Couette flow and the Poiseuille flow away from the wall—in a domain located symmetrically around the axis, which is called the core region—show behavior similar to free turbulent flows. Therefore the DQTM is identically applied as in free turbulent shear flows. The results for plane Couette flow [11] reveal a complete order/disorder description of turbulence, well known from other statistical systems showing critical phenomena (see, e.g., Ref. [12]).

II. THE BASIC EQUATIONS

The basic equations of incompressible turbulent flow problems can be derived from the Navier-Stokes equations. They are called Reynolds equations. For the plane case of Poiseuille flow (see Fig. 1)—together with the continuity equation—the momentum equations are the following (see Ref. [5] resuming work performed by Pai [13])

$$\frac{\partial \overline{u_1}}{\partial x_1} = 0, \tag{1a}$$

$$\frac{1}{\rho}\frac{\partial \overline{p}}{\partial x_1} - \nu \frac{\partial^2 \overline{u_1}}{\partial x_2^2} + \frac{\partial \overline{u_2' u_1'}}{\partial x_2} = 0, \tag{1b}$$

*Present address: Daimler-Chrysler Research and Technology, P.O. Box 2360, D-89013 Ulm, Germany.

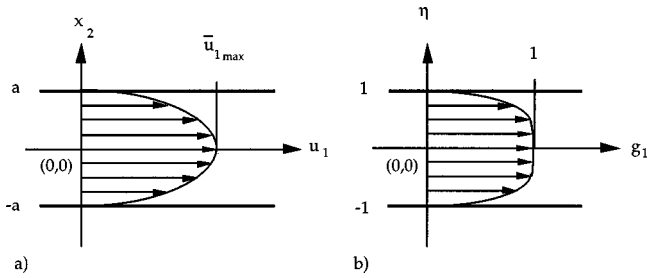

FIG. 1. Laminar and turbulent Poiseuille flow between two plane parallel plates. In the laminar case, the velocity profile is known to be of parabolic type (a). In turbulent regimes with increasing Reynolds number, the mean velocity profiles flatten (b). In the figure on the right, dimensionless variables have been used.

$$\frac{1}{\rho}\frac{\partial \overline{p}}{\partial x_2}+\frac{\partial \overline{(u_2')^2}}{\partial x_2}=0. \tag{1c}$$

$\overline{u_i}$ denotes the mean velocity component in space direction $\mathbf{e}_i$, presented by the corresponding coordinate axis with values x_i. The coordinate x_1 denotes the downstream direction and x_2 denotes the direction perpendicular to the walls. The time-averaged physical quantities, characterized by an overbar, are functions of space only. $\overline{p}$ is the mean pressure and ν the kinematic viscosity of the fluid, whereas ρ denotes the constant density of the incompressible fluid. Here second-order correlations occur, containing the fluctuation velocities u_i'.

We now briefly recall some considerations, which are important for the understanding of this theory. From Eq. (1a) it is evident that the time-averaged velocity in the downstream direction

$$\overline{u_1}=\overline{u_1}(x_2) \tag{2}$$

only depends on x_2. Dimensionless space coordinates are introduced

$$\xi=\frac{x_1}{a}, \tag{3a}$$

$$\eta=\frac{x_2}{a}. \tag{3b}$$

Furthermore, the following characteristic velocity is defined:

$$u^*=\sqrt{\frac{|\tau_0|}{\rho}}, \tag{4a}$$

$$\tau_0=\pm\mu\left.\frac{\partial \overline{u_1}}{\partial x_2}\right|_{\pm a}, \tag{4b}$$

where the near-wall shear stress τ_0 has been introduced (e.g., see Ref. [14]). The characteristic quantities introduced so far are linked to the two Reynolds numbers

$$\mathrm{Re}=\frac{\overline{u}_{1_{\max}}a}{\nu}, \tag{5a}$$

$$\mathrm{Re}^*=\frac{u^*a}{\nu}\Rightarrow \mathrm{Re}=\frac{\overline{u}_{1_{\max}}}{u^*}\mathrm{Re}^*. \tag{5b}$$

In this paper the following self-similar functions are made use of:

$$f_1(\eta,\mathrm{Re}^*)=\frac{\overline{u_1}}{u^*}, \tag{6}$$

$$P(\xi,\eta,\mathrm{Re}^*)=\frac{\overline{p}-\overline{p_0}}{\rho u^{*2}}, \tag{7}$$

$$f_{21}(\eta,\mathrm{Re}^*)=\frac{\overline{u_2'u_1'}}{u^{*2}}, \tag{8}$$

$$f_{22}(\eta,\mathrm{Re}^*)=\frac{\overline{(u_2')^2}}{u^{*2}}. \tag{9}$$

It can be seen that not only f_1, but also f_{21} and f_{22}, are independent of ξ. By applying Eq. (6) to Eq. (9), we obtain the following two differential equations:

$$\frac{\partial P}{\partial \xi}-\frac{1}{\mathrm{Re}^*}\frac{\partial^2 f_1}{\partial \eta^2}+\frac{\partial f_{21}}{\partial \eta}=0 \tag{10}$$

and

$$\frac{\partial P}{\partial \eta}+\frac{\partial f_{22}}{\partial \eta}=0. \tag{11}$$

The boundary conditions are the following:

$$f_\gamma(-1,\mathrm{Re}^*)=f_\gamma(+1,\mathrm{Re}^*)=0,\qquad \gamma\in\{1,21,22\}. \tag{12}$$

In consistency with Eq. (7), it is possible to fix the pressure

$$P(0,-1,\mathrm{Re}^*)=0. \tag{13}$$

From Eqs. (10) and (11) linear relationships are obtained

$$(P+f_{22})=A(\mathrm{Re}^*)\xi+C(\mathrm{Re}^*), \tag{14}$$

$$\frac{1}{\mathrm{Re}^*}\frac{\partial f_1(\eta,\mathrm{Re}^*)}{\partial \eta}-f_{21}(\eta,\mathrm{Re}^*)-A(\mathrm{Re}^*)\eta-B(\mathrm{Re}^*)=0. \tag{15}$$

The total shear stress τ_{tot} is given by the viscous τ_0 and the turbulent shear stress or Reynolds shear stress τ_t,

$$\tau_{\mathrm{tot}}=\tau_0+\tau_t=\mu\frac{\partial \overline{u_1}}{\partial x_2}-\rho\overline{u_2'u_1'}. \tag{16}$$

Near the wall, the turbulent fluctuations disappear

$$\left.\frac{\tau_{\mathrm{tot}}}{\rho}\right|_{\pm a}=\mp(u^*)^2 \tag{17a}$$

$$=\nu\left.\frac{\partial \overline{u_1}}{\partial x_2}\right|_{\pm a} \tag{17b}$$

which yields

$$\left.\frac{df_1}{d\eta}\right|_{\pm 1} = \mp \mathrm{Re}^*. \tag{17c}$$

Substituting obtained results into Eq. (15), it follows that

$$\pm A + B = \mp 1. \tag{18}$$

By solving this system of two equations of two variables it is found that $A=-1$ and $B=0$. Therefore, Eqs. (14) and (15) change to

$$P(\xi,\eta,\mathrm{Re}^*) + f_{22}(\eta,\mathrm{Re}^*) + \xi = 0, \tag{19}$$

$$\frac{1}{\mathrm{Re}^*}\frac{\partial f_1(\eta,\mathrm{Re}^*)}{\partial \eta} - f_{21}(\eta,\mathrm{Re}^*) + \eta = 0. \tag{20}$$

The integration of Eq. (20) produces the main equation before introducing any turbulence modeling

$$f_1(\eta,\mathrm{Re}^*) = \mathrm{Re}^*\left[\tfrac{1}{2}(1-\eta^2) + \int_{-1}^{\eta} f_{21}(\theta,\mathrm{Re}^*)\,d\theta\right]. \tag{21}$$

To fulfill the boundary conditions in the laminar case ($f_{21}=0$), in Eq. (21) we set the integration constant equal to $\frac{1}{2}$. Now, the velocity profile in laminar flow describes the parabolic Hagen-Poiseuille profile

$$f_1(\eta,\mathrm{Re}^*) = \frac{\mathrm{Re}^*}{2}(1-\eta^2). \tag{22}$$

III. CONSERVED MOMENTUM AND THE DIFFERENCE-QUOTIENT TURBULENCE MODEL

The application of any turbulence model is still an empirical procedure because of a lacking proof of the validity of the closure technique in general. Therefore, an explanation in terms of fluid dynamics of the DQTM at present is rather based on physical intuition than first physical principles. To give some convincing explanations, at the beginning we follow simple arguments of Prandtl, which can be found in most textbooks on turbulence, e.g., [5,14–17], etc. As a fluid is in turbulent motion, it carries fluid elements from place to place. A control volume of fluid—small compared with the Kolmogorov microscale, but large in comparison with the molecular scale—is gradually transported away from its initial location (see Fig. 2).

At time $t=0$ each of the two selected mass elements A and B are considered to be contained in spherical elements of equal size. A is positioned on the center line ($x_2=0$) and B is located very close to the upper boundary plate ($x_2=a$). The chosen elements are much smaller than shown in Fig. 2. Therefore, for simplicity fluid parcel B is assumed to be exactly at $x_2=a$. The opposite motion of A from the center line to the boundary and that of B in the reverse direction guarantee mass conservation. Now the wandering of fluid element A is investigated. By turbulent motion it is transported to the position x_2^*. Prandtl assumed a small mixing length to be the characteristic distance over which the momentum is conserved. In contrast, in this model the eddies conserve momentum over much larger distances, e.g., in this specific case it is as long as l_A. Nowadays it is known that a fluid lump is dispersed ever so rapidly. Particles, which are initially neighbors, are exponentially separated. This clearly demonstrates the limited character of this model. Still, the rough assumptions lead to a prediction of the correct mean momentum transfer (see below). The averaged excess momentum at the new position is

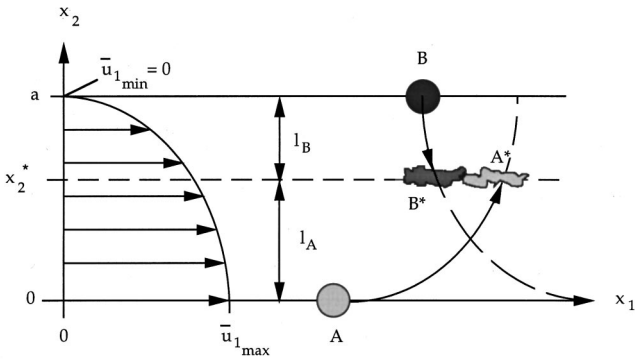

FIG. 2. Geometry of intercollision of fluid lumps. This figure has been copied from Ref. [5] and adapted to the new ideas leading to the DQTM. An initially spherical element A (or B) is transported and simultaneously elongated to become A^* (respectively, B^*).

$$\overline{\Delta M} = \rho\overline{\{[\overline{u_1}(0)+u_1'(0)]-[\overline{u_1}(x_2^*)+u_1'(x_2^*)]\}}$$

$$= \rho[\overline{u_1}(0)-\overline{u_1}(x_2^*)], \tag{23}$$

because the time averages of the fluctuations vanish per definition.

The volume flux density is amplified by a length ratio [18]

$$j_2(x_2^*) = \frac{a}{x_2^*}u_2(x_2^*). \tag{24}$$

The root mean square velocity of u_2 is

$$\sqrt{\overline{u_2^2}} = \sqrt{\overline{(\overline{u_2}+u_2')^2}} \tag{25a}$$

$$= \sqrt{\overline{u_2'^2}}, \tag{25b}$$

because $\overline{u_2}$ is zero. The turbulent shear stress is defined by

$$\tau_t = -\overline{j_2 \Delta M}. \tag{26}$$

By applying Eqs. (24) and (25b) one obtains

$$\tau_t = -c\frac{a}{x_2^*}\sqrt{\overline{u_2'^2}}\;\overline{\Delta M}, \tag{27}$$

with a correlation coefficient $0 \leqslant c \leqslant 1$. A further model assumption is that this correlation is very strong and therefore we can set $c=1$. If a high number of tracer particles is injected in the turbulent flow, e.g., at the origin of the coordinate system, in the mean the contaminated region shows a

continuous spreading. The half-width of this region is described by a function $b(x_1)$. In a linear approximation it follows that

$$\sigma = \frac{db}{dx_1} \tag{28a}$$

$$= \tan\frac{\alpha}{2} \tag{28b}$$

$$= \frac{\sqrt{\overline{u_2^2}}}{\sqrt{\overline{u_1^2}}} \tag{28c}$$

$$= \frac{\sqrt{\overline{u_2'^2}}}{\sqrt{\overline{u_1^2}+\overline{u_1'^2}}} \tag{28d}$$

$$\cong \frac{\sqrt{\overline{u_2'^2}}}{\overline{u_1}} \tag{28e}$$

$$|\overline{u_1}| \gg \sqrt{\overline{u_1'^2}}, \tag{28f}$$

where σ denotes the spreading parameter and α the spreading angle. In Poiseuille flow the spreading by turbulent convection is only a flow internal feature, where in a jet flow it also defines the boundary of the turbulent domain. The turbulence intensities are assumed to be small compared with the mean downstream velocity [see Eq. (28f)]. From Eq. (27) by substituting (28e) one obtains

$$\tau_t = -\rho\sigma\chi_2\overline{u}_1(x_2^*)\frac{\overline{u}_1(0)-\overline{u}_1(x_2^*)}{x_2^*}. \tag{29}$$

We already have noted that the quantity χ_2 denotes a characteristic length in the x_2 direction (in Poiseuille flow it is equal to the width a). To fulfill Galilean invariance $x_{2\,\max}=0$ and $\overline{u}_{1\,\min}=0$ are added. The quantity $x_{2\,\max}$ denotes the location where the mean downstream velocity is maximal. The model ideas can be applied to different locations downstream and to every position in the perpendicular direction. Therefore, we can introduce the variable x_1, and we can also omit the asterisk in x_2^*,

$$\tau_t = \rho\sigma\chi_2[\overline{u}_1(x_1,x_2)-\overline{u}_{1\,\min}(x_1)] \times\frac{\overline{u}_{1\,\max}(x_1)-\overline{u}_1(x_1,x_2)}{x_{2\,\max}-x_2}, \tag{30}$$

which finally defines the DQTM, as it was introduced in several previous papers without much explanation. It must be remarked that in the limit x_2 toward zero the excess momentum vanishes and a generalized eddy viscosity (see Sec. IX) increases to infinity. The product correctly gives a finite limiting value, which corresponds to the correct turbulent shear stress as it is experimentally observed.

IV. SPECIAL CASES: THE MODELS OF PRANDTL

Applying a Taylor expansion in Eq. (30) from location x_2 to derive $\overline{u}_{1\,\max}$ over the the distance $l_A=(x_{2\,\max}-x_2)$, the zero-order terms drop out, and one obtains

$$\tau_t = \rho\sigma\chi_2(\overline{u}_1-\overline{u}_{1\,\min})\frac{\partial\overline{u}_1}{\partial x_2}. \tag{31}$$

With $\chi_2=b$ and a substitution of the first mean velocity by its maximal value Prandtl's *free shear layer model* is obtained [19]

$$\tau_t = \sigma\rho b(\overline{u}_{1\,\max}-\overline{u}_{1\,\min})\frac{\partial\overline{u}_1}{\partial x_2}. \tag{32}$$

Stepping back to Eq. (31) and also expanding $\overline{u}_{1\,\min}$ in the remaining velocity difference leads to

$$\tau_t = \rho l^2\left\{\overline{\left[\left(\frac{\partial\overline{u}_1}{\partial x_2}\right)+l'\left(\frac{\partial^2\overline{u}_1}{\partial x_2^2}\right)\right]^2}\right\}^{1/2}\frac{\partial\overline{u}_1}{\partial x_2}, \tag{33}$$

where a mean gradient over a distance l' has been introduced, and the relations $\chi_2=l_B=l$ have been applied. Prandtl assumed that in the positive and negative x_{2-} direction the second mixing length l' is statistically equally distributed, so that in the procedure transforming Eq. (33) to Eq. (34), the cross terms cancel out,

$$\tau_t = \rho l^2\left\{\left(\frac{\partial\overline{u}_1}{\partial x_2}\right)^2+l'^2\left(\frac{\partial^2\overline{u}_1}{\partial x_2^2}\right)^2\right\}^{1/2}\frac{\partial\overline{u}_1}{\partial x_2}. \tag{34}$$

In this *mean-gradient theory* we have written l'^2 instead of $\overline{l'^2}$. When l' is assumed to be zero only first-order derivatives remain,

$$\tau_t = \rho l^2\left|\frac{\partial\overline{u}_1}{\partial x_2}\right|\frac{\partial\overline{u}_1}{\partial x_2}. \tag{35}$$

Finally we have obtained the simplest but the most widely applied model of the numerous approaches that Prandtl has proposed [6]. It is named the *mixing-length model*. The development of his models went in the opposite direction [from Eq. (35) in the year 1925 to Eq. (32) in 1942]. Because of insufficiencies of the mixing-length model, e.g., deviations of calculated results and experimental data at points of vanishing derivatives of the mean downstream velocity, Prandtl gradually improved his gradient theory. From the presentation here, it can be seen how closely his theories approach the DQTM. To make this even clearer the model (32) can be slightly rewritten

$$\tau_t = \sigma\rho b^2\frac{\partial\overline{u}_1}{\partial x_2}\frac{\overline{u}_{1\,\max}-\overline{u}_{1\,\min}}{b}. \tag{36}$$

In the free shear flow model Prandtl obtained a difference quotient, which spans the whole turbulent region. But on the other hand, the expression in front of the difference quotient, which also defines a modified eddy diffusivity [20], is still a local quantity. There exist many critics of gradient-type, respectively, eddy diffusivity models (e.g., see Ref. [21]). In a textbook on turbulence [17] one finds the following state-

ments: ''We have to conclude that the truncation of the Taylor series expansion involved in (here a formula of the eddy viscosity concept occurs) is not justified. Therefore, a gradient-transport model, which links the stress to the rate of strain at the same point in time and space, cannot be used for turbulent flows.'' Note that this criticism does not apply to the DQTM.

V. THE BASIC EQUATION OF TURBULENT POISEUILLE FLOW

Omitting the dependency on the variable x_1 again [compare with statement of Eqs. (1a) and (2)] in dimensionless form we have

$$f_{21}(\eta)=\sigma\frac{1}{\eta}f_1(\eta)[f_1(0)-f_1(\eta)]. \tag{37}$$

Inserting this expression into Eq. (21) leads to an integral equation. It is more convenient, however, to substitute the right-hand side of Eq. (37) into Eq. (20), which gives the following differential equation:

$$\frac{1}{\mathrm{Re}^*}f_1'(\eta)-\sigma\frac{1}{\eta}f_1(\eta)[f_1(0)-f_1(\eta)]+\eta=0, \tag{38a}$$

$$'\equiv\frac{d}{d\eta}. \tag{38b}$$

After having dropped Eq. (19), we now only consider this basic equation. We may therefore introduce the total derivative. By further introducing the following functions:

$$g_1(\eta)=\frac{f_1(\eta)}{f_1(0)}, \tag{39a}$$

$$g_{21}(\eta)=f_{21}(\eta) \tag{39b}$$

and the abbreviations

$$\alpha=\frac{f_1(0)}{\mathrm{Re}^*}, \tag{40a}$$

$$\beta=\sigma f_1(0)^2, \tag{40b}$$

the differential equation of the problem is obtained

$$\alpha\eta g_1'(\eta)-\beta g_1(\eta)+\beta g_1(\eta)^2+\eta^2=0. \tag{41}$$

A symmetry condition and the boundary conditions are the following:

$$g_1(\eta)=g_1(-\eta), \tag{42a}$$

$$g_1(0)=1, \tag{42b}$$

$$g_1(1)=0. \tag{42c}$$

From Eqs. (17c) and (39a) it can be concluded that

$$\left.\frac{dg_1}{d\eta}\right|_{\pm1}=\mp\frac{\mathrm{Re}^*}{f_1(0)} \tag{43a}$$

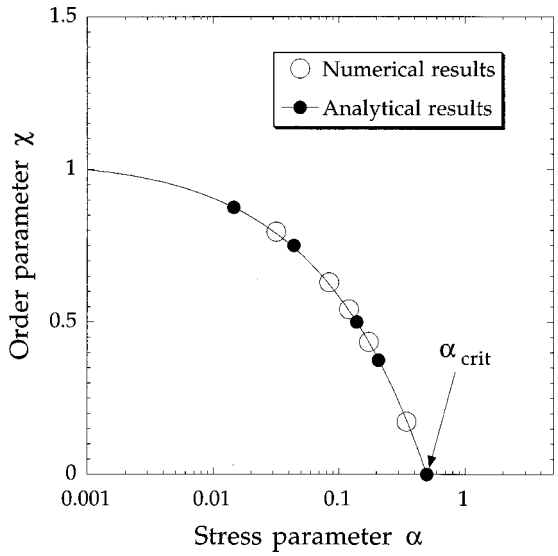

FIG. 3. Analytically and numerically derived functional relation between the stress parameter α, which is inversely connected to the Reynolds number Re* by Eqs. (43a) and (43b), and β, respectively, the order parameter χ. Corresponding mean velocity profiles and Reynolds stresses are shown in Fig. 4.

$$=\mp\frac{1}{\alpha}, \tag{43b}$$

which means that the slope of the time-averaged velocity profile near the plane plate is directly proportional to the Reynolds number Re*. This is in qualitative agreement with experimental observations of a decreasing boundary layer thickness in terms of an increasing Reynolds number.

Running a numerical calculation scheme, starting at $\eta=-1$, for a certain quantity β, one has to choose the parameter α so that the profile hits $(\eta,g)=(+1,0)$ on the opposite side and thereby fulfills the boundary condition (42). The function

$$\chi=\frac{\beta}{4}, \tag{44}$$

which has been evaluated by this procedure, is shown in Fig. 3 and is compared with analytical results of Sec. VI.

If $\alpha\to0$ then—just as in plane Couette flow [11]—β is equal to four, and χ identical to one. From numerical calculations it follows that β is positive and smaller than or equal to four. This upper limit will be shown analytically to be correct. Because of Eq. (42a) it is sufficient to study the behavior of g_{21} in the interval $0\leqslant\eta\leqslant1$. From Eqs. (20), (38a), (38b), (39a), (39b), and (42a)–(42c), we may conclude that

$$\alpha\frac{dg_1(\eta)}{d\eta}=g_{21}(\eta)-\eta\leqslant0 \tag{45}$$

and

$$g_{21}=\beta\frac{1}{\eta}g_1(1-g_1), \tag{46}$$

and by substituting Eq. (46) into Eq. (45), we obtain

$$\beta g_1(1-g_1)\leqslant\eta^2\leqslant 1, \quad \forall\,\eta\in[0,1]\Rightarrow\beta\leqslant 4. \tag{47}$$

Substituting the DQTM into the Navier-Stokes equation and solving it together with the continuity equation yields an order/disorder description of turbulence, with several analogies in other fields where statistical physics applies. The two phases are laminar domains and turbulent patches. Considering decreasing values for α at $\alpha_{\text{crit}}=0.5$, the laminar flow—characterized by $\chi=0$—becomes unstable and the turbulent domains grow (see Fig. 3). At $\alpha=0$ (infinite Reynolds number) no laminar interspaces remain and the most irregular turbulent flow, showing the highest order $\chi=1$, is obtained. In Ref. [11] a suitable physical quantity is shown to be related to the order parameter χ.

VI. ANALYTICAL SOLUTIONS FOR LOW, MODERATE, AND HIGH REYNOLDS NUMBERS

Equation (41) with the requirements (42a)–(42c) can be analytically solved. Three cases are distinguished. The third case will mainly be the subject of the next section. In this section, the simplest of these problems is considered first,

$$\beta=0\Rightarrow\alpha=\tfrac{1}{2}\Rightarrow g(\eta)=1-\eta^2. \tag{48}$$

This is the case that describes laminar flows at Reynolds numbers up to the critical value.

More effort is needed to solve the second case, i.e., the flow problems for finite Reynolds numbers above the critical value, thus $\beta>0$ and $\alpha>0$. The following functional relation is considered:

$$g_1=H\frac{h'}{h}, \tag{49}$$

with

$$H=\frac{\alpha}{\beta}\eta. \tag{50}$$

Equation (41) can be transformed into a Bessel-type equation

$$\alpha^2\eta h''+(\alpha^2-\alpha\beta)h'+\beta\eta h=0. \tag{51}$$

Applying the variable transformation

$$\psi=\lambda\eta \tag{52}$$

together with

$$\lambda=\frac{\sqrt{\beta}}{\alpha} \tag{53}$$

leads to

$$\psi\frac{\partial^2 h}{\partial\psi^2}+\left(1-\frac{\beta}{\alpha}\right)\frac{\partial h}{\partial\psi}+\psi h=0. \tag{54}$$

According to Ref. [22], the solution of Eq. (51) is

$$h(\psi)=\psi^{\kappa}C_{\kappa}(\tilde{\lambda}\psi) \tag{55a}$$

where

$$\kappa=\frac{\beta}{2\alpha}, \quad \tilde{\lambda}^2=1, \text{ and } C\in\{J,Y\}. \tag{55b}$$

J denotes the Bessel functions and Y the Weber functions. Furthermore, from Eqs. (40) one derives [see (43b)]

$$\sigma=\frac{\beta}{f_1(0)^2}=\frac{\beta}{\alpha^2\,\text{Re}^{*2}}=\beta\left(\frac{u^*}{\overline{u}_{1_{\max}}}\right)^2. \tag{56}$$

By substituting the right-hand terms of Eq. (40) into Eq. (55), an expression for κ can be derived

$$\kappa=\frac{\beta}{2\alpha}=\frac{1}{2}\sigma\,\text{Re}^*\frac{\overline{u}_{1_{\max}}}{u^*}=\frac{1}{2}\sigma\,\text{Re}. \tag{57}$$

Continuing with Eq. (55), the following four equations exist to construct solutions:

$$h_1(\psi)=\psi^{\kappa}J_{\kappa}(\psi), \tag{58a}$$

$$h_2(\psi)=\psi^{\kappa}J_{\kappa}(-\psi), \tag{58b}$$

$$h_3(\psi)=\psi^{\kappa}Y_{\kappa}(\psi), \tag{58c}$$

$$h_4(\psi)=\psi^{\kappa}Y_{\kappa}(-\psi). \tag{58d}$$

Bessel functions of the first type and Weber functions, which are Bessel functions of the second type—having negative arguments—are more difficult to apply. By introducing an analytic continuation, they can be reduced to the functions with positive arguments [22]

$$h_2(\psi)=e^{i\kappa\pi}h_1(\psi), \tag{59a}$$

$$h_4(\psi)=e^{-i\kappa\pi}h_3(\psi)+2i\sin(\kappa\pi)\cot(\kappa\pi)h_1(\psi) \tag{59b}$$

for rational κ and

$$h_2(\psi)=(-1)^n h_1(\psi), \tag{60a}$$

$$h_4(\psi)=(-1)^n h_3(\psi)+2i(-1)^n h_1(\psi) \tag{60b}$$

when κ is an integer number $\kappa=n$. The general solution for h can be written as a linear combination of h_1 and h_3,

$$h=p\psi^{\kappa}J_{\kappa}(\psi)+q\psi^{\kappa}Y_{\kappa}(\psi). \tag{61}$$

The derivative is

$$\frac{dh}{d\psi}=p\psi^{\kappa}J_{\kappa-1}(\psi)+q\psi^{\kappa}Y_{\kappa-1}(\psi). \tag{62}$$

Together with Eqs. (49) and (52) we obtain

$$g_1(\psi)=\frac{1}{2\kappa}\psi\frac{pJ_{\kappa-1}(\psi)+qY_{\kappa-1}(\psi)}{pJ_{\kappa}(\psi)+qY_{\kappa}(\psi)}. \tag{63}$$

This equation has to fulfill the requirement (42b)

$$\lim_{\psi\to 0} g_1(\psi)=1. \tag{64}$$

We conclude from Eq. (64) that

$$q=0. \tag{65}$$

Thus

$$g_1(\psi)=\frac{\psi}{2\kappa}\frac{J_{\kappa-1}(\psi)}{J_\kappa(\psi)} \tag{66a}$$

$$=\frac{J_{\kappa-1}(\psi)}{J_{\kappa-1}(\psi)+J_{\kappa+1}(\psi)} \tag{66b}$$

is obtained. The requirement Eq. (42c) yields

$$J_{\kappa-1}\left(\frac{\sqrt{\beta}}{\alpha}\right)=0, \tag{67}$$

and the argument of Eq. (67) has to be $j_{\kappa-1,1}$, i.e., the first zero of the Bessel function $J_{\kappa-1}$. From

$$\frac{\sqrt{\beta}}{\alpha}=j_{\kappa-1,1} \tag{68a}$$

and

$$2\kappa=\frac{\beta}{\alpha}, \tag{68b}$$

it follows that

$$\alpha=\frac{2\kappa}{(j_{\kappa-1,1})^2} \tag{69a}$$

and

$$\beta=\frac{4\kappa^2}{(j_{\kappa-1,1})^2}. \tag{69b}$$

In this way, for a given value $\kappa\in\mathbb{R}^+$, pairs (α,β) can be calculated by means of tables and formulas presented in Ref. [22]. From this reference, we also find that

$$J_\kappa(\psi)=\left(\frac{\psi}{2}\right)^\kappa\sum_{k=0}^{\infty}\frac{\left(-\frac{\psi^2}{4}\right)^k}{k!\Gamma(\kappa+k+1)}. \tag{70}$$

For negative arguments, ψ, instead of Eq. (66a), the following calculation must be performed:

$$g_1(\psi)=\frac{1}{\kappa}\frac{\sum_{k=0}^{\infty}\frac{\left(-\frac{\psi^2}{4}\right)^k}{k!\Gamma(\kappa+k)}}{\sum_{k=0}^{\infty}\frac{\left(-\frac{\psi^2}{4}\right)^k}{k!\Gamma(\kappa+k+1)}}. \tag{71}$$

With Eq. (71) the symmetry of $g_1(\psi)$ according to Eq. (42a) is guaranteed. From Eqs. (46) and (66b) it follows that the scaled Reynolds shear stress is (see Fig. 4)

$$g_{21}=\beta j_{\kappa-1,1}\frac{1}{\psi}\frac{J_{\kappa-1}J_{\kappa+1}}{(J_{\kappa-1}+J_{\kappa+1})^2}. \tag{72}$$

The third case, where $\beta\to 4$ and therefore $\alpha\to 0$, is easy to solve. The differential equation (41) reduces to a normal quadratic equation. By taking the boundary condition (42) into account, it is solved by

$$g_1=\frac{1}{2}(1+\sqrt{1-\eta^2}). \tag{73}$$

In the next section it is shown that Eq. (73) is in fact the pointwise limit of solutions (66a) and (66b) for $\kappa\to\infty$.

VII. THE INFINITE REYNOLDS NUMBER SOLUTION

Studying the time-averaged velocity profiles—from Eqs. (66a) and (70)—we conclude that

$$g_1(\eta)=\frac{\eta}{\sqrt{\beta}}\frac{J_{\kappa-1}\left(\frac{2\kappa}{\sqrt{\beta}}\eta\right)}{J_\kappa\left(\frac{2\kappa}{\sqrt{\beta}}\eta\right)}. \tag{74}$$

The behavior of Eq. (74) is considered in the limit $\kappa\to\infty$. This corresponds to the limit $\beta\to 4$. It will be shown that Eq. (74) tends pointwise toward solution (73) if $|\eta|<1$. Due to Eq. (42a) it can be assumed that $\eta\geqslant 0$. To calculate the limit it can be set

$$\frac{2\eta}{\sqrt{\beta}}=\mathrm{sech}(\gamma_1)=\frac{1}{\cosh(\gamma_1)} \tag{75}$$

for some γ_1, since the first term in Eq. (75) is assumed to be smaller or equal to one. The behavior of

$$J_\kappa\left(\frac{2\kappa}{\sqrt{\beta}}\eta\right) \tag{76}$$

in the limit $\kappa\to\infty$ can be found in [22]. Some care is needed, however, when determining the same limit for

$$J_{\kappa-1}\left(\frac{2\kappa}{\sqrt{\beta}}\eta\right). \tag{77}$$

Since the inequality

$$\frac{2\kappa\eta}{(\kappa-1)\sqrt{\beta}}=\frac{2\eta}{\sqrt{\beta}}\frac{\beta}{\beta-2\alpha}<1 \tag{78}$$

can be assumed, we can set

$$\frac{2\kappa\eta}{(\kappa-1)\sqrt{\beta}}=\mathrm{sech}(\gamma_2) \tag{79}$$

for some γ_2. We make use of [22] to obtain

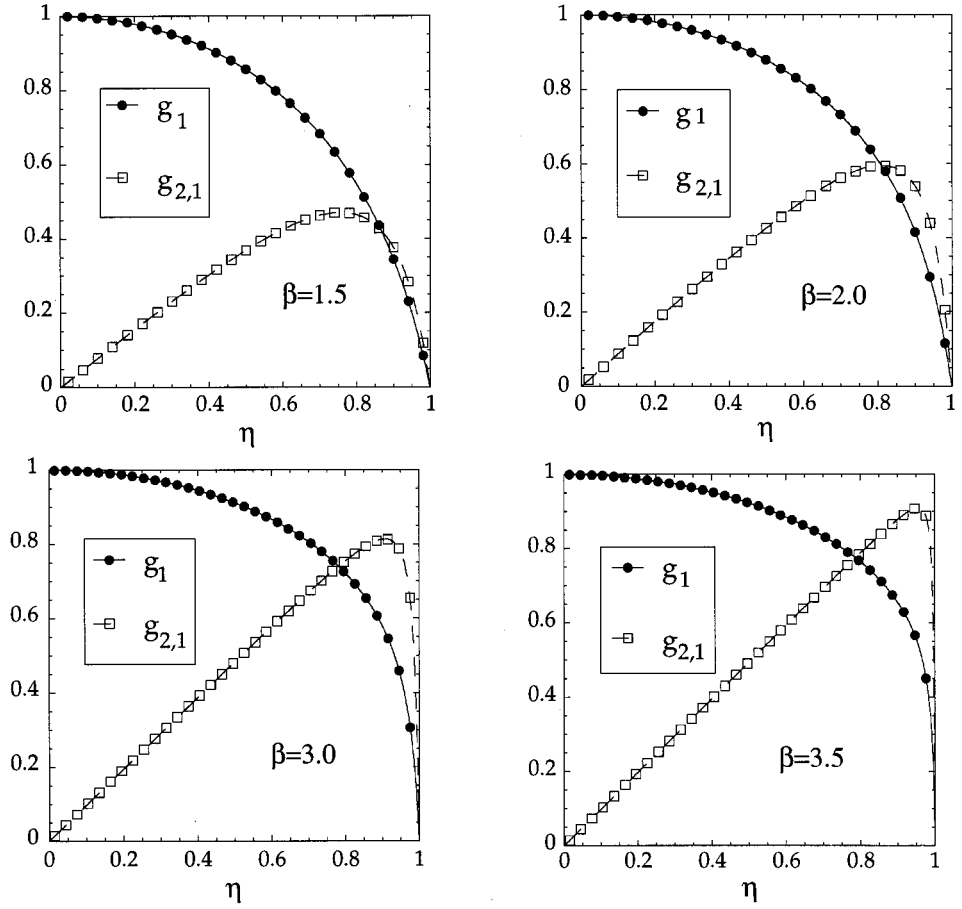

FIG. 4. Four time-averaged velocity profiles g_1 and Reynolds shear stresses g_{21} for different turbulence intensities $\beta(0\leqslant\beta\leqslant 4)$. With increasing parameter β, the time-averaged velocity profiles flatten, and the Reynolds shear stresses converge toward a triangle-type profile.

$$J_\kappa[\kappa\,\mathrm{sech}(\gamma_{12})]\rightarrow\frac{\exp\{\kappa[\tanh(\gamma_{12})-\gamma_{12}]\}}{\sqrt{2\pi\kappa\tanh(\gamma_{12})}}\quad\text{if}\quad\kappa\rightarrow\infty, \tag{80}$$

with

$$\gamma_{12}=\log\left[\frac{1}{\mathrm{sech}(\gamma_{12})}+\sqrt{\frac{1}{\mathrm{sech}^2(\gamma_{12})}-1}\right], \tag{81a}$$

$$\tanh(\gamma_{12})=\sqrt{1-\mathrm{sech}^2(\gamma_{12})}. \tag{81b}$$

We have

$$\mathrm{sech}(\gamma_2)-\mathrm{sech}(\gamma_1)=\frac{1}{\kappa}\mathrm{sech}(\gamma_2), \tag{82a}$$

$$\frac{\mathrm{sech}(\gamma_1)}{\mathrm{sech}(\gamma_2)}=1-\frac{1}{\kappa} \tag{82b}$$

and

$$\tanh(\gamma_2)-\tanh(\gamma_1)=-\frac{\mathrm{sech}(\gamma_1)\mathrm{sech}(\gamma_2)}{\sqrt{1-\mathrm{sech}^2(\gamma_1)}}\frac{1}{\kappa}+O(\kappa^{-2}). \tag{83}$$

Inserting Eq. (80) into Eq. (74) and taking into account Eqs. (80)–(82) and

$$\exp[\kappa(\gamma_1-\gamma_2)]=\left[1+\frac{1}{\kappa}\frac{1}{\sqrt{1-\mathrm{sech}^2(\gamma_2)}}+O(\kappa^{-2})\right]^\kappa\xrightarrow[\kappa\rightarrow\infty]{}\exp\left(\frac{1}{\sqrt{1-\mathrm{sech}^2(\gamma_2)}}\right), \tag{84}$$

we obtain, by using

$$\lim_{\kappa\rightarrow\infty}\gamma_1=\lim_{\kappa\rightarrow\infty}\gamma_2, \tag{85}$$

relations that are finite, the final result obtained in the infinite Reynolds number limit [compare with Eq. (73)]

$$g_1=\frac{1+\sqrt{1-\eta^2}}{2}. \tag{86}$$

Rearranging the equation and substituting

$$\zeta=2g_1-1, \tag{87}$$

we obtain

$$\zeta^2+\eta^2=1, \tag{88}$$

which is the equation describing the unit circle. Figure 5(a) shows the time-averaged velocity profile of a horizontal flow arriving from the left and leaving toward the right. In Fig. 5(b) the corresponding Reynolds shear stress is plotted.

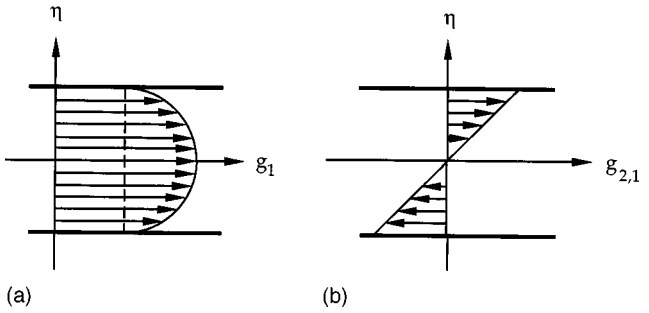

FIG. 5. The time-averaged velocity profile of infinite Reynolds number flow contains a semicircle on top of a rectangle (a). The second figure (b) is the corresponding Reynolds shear stress, which is of triangular type. The two mean profiles are of elementary geometric nature.

By inserting Eq. (86) into Eq. (46) with $\beta=4$ the Reynolds shear stress is calculated

$$g_{21}=4\frac{1}{\eta}\frac{1+\sqrt{1-\eta^2}}{2}\left(1-\frac{1+\sqrt{1-\eta^2}}{2}\right)$$

$$=\frac{1}{\eta}(1+\sqrt{1-\eta^2})(1-\sqrt{1-\eta^2})=\eta, \tag{89}$$

thus a linear dependence on η if $|\eta|<1$ [since the derivation of Eq. (86) was based on this assumption]. This antisymmetric function partly represents a double triangle. A more sophisticated treatment is based on the mathematical theory of distributions. Then the solution for the Reynolds stress additionally fulfills the equations $g_{21}(-1)=g_{21}(1)=0$.

VIII. COMPARISON WITH EXPERIMENTAL RESULTS

A first statement of the presented theory—which needs to be examined carefully—is that the time-averaged velocity profiles for high Reynolds numbers converge toward a semicircle. Experimental data are given, for example, by Laufer [23] and Reichhardt [24]. Although the data of Laufer confirm the presented theoretical results very well, for the mean velocity profile the measurements of Reichhardt are chosen for comparison (see Fig. 6).

The experiments confirm the model results convincingly. But the good results are a little misleading. In the domain surrounding $\eta=\pm 0.6$ some measured quantities are somewhat smaller than the functional values. On the other hand, exactly there—when the excitation of the flow system is further increased—the mean velocity profiles begin to exceed the theoretical functions. The reason leading to this statement is complex and discussed in the remaining part of this section.

The ''Princeton super pipe data'' [25] represent the newest results of the axisymmetric Poiseuille flow measured at hitherto highest Reynolds numbers, for example, Re $=17\,629\,500$. The mean velocity profile between $\eta=-0.5$ and $\eta=0.5$ also follows the circle profile with a maximum relative error of 1.2%. Only in the turbulent boundary layer, at larger absolute values of η, the relative deviation takes higher values. From theory and experiments it is known that

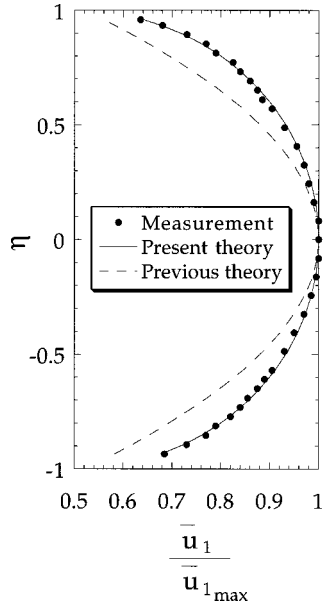

FIG. 6. The measured time-averaged velocity profile for fully developed turbulent flow with $u^*=15.2$ cm/s (from Ref. [24]) compared with the circle solution, denoted by ''present theory.'' The measurements were performed in a channel with height 24.6 cm, which is shown after applying a scaling as $\eta=[-1,1]$. The width of the channel is 98 cm. A former model, referred to in Ref. [24], leads to a result of parabolic type (see ''previous theory'').

in the boundary layer, closer to the wall, the results of pipe and channel flow are practically identical. A comparison of experimental results of boundary-layer flow and pipe flow is presented in Ref. [26]. Therefore, in this domain equal behavior must be expected for flows in plane channels and axisymmetric flows in pipes. So also in the plane case, at higher Reynolds numbers, it is expected that the experimental values could exceed the theoretical ones shown in Fig. 6. But the solutions in the core region, which is roughly defined by the interval $-0.5<\eta<0.5$, hardly alter anymore when the excitation is further increased. Therefore, in Fig. 6 only in the core region the agreement between theory and experiment is reliable.

A further crucial test of the theory is a comparison of the calculated Reynolds stress with experimental data (see Fig. 7). The theoretical results are again in good agreement with the experimental data set. The deviations from the infinite Reynolds number solution are exactly as expected from the calculations leading to Fig. 4.

IX. CRITICAL CONCLUSIONS

It is assumed that the theory presented is valid in a region of about one-half the distance between the plates located symmetrically to the center line. This region is named the core region (see Fig. 8). That the theory does not apply to the neighboring boundary layer can be seen by the following arguments. Turbulent fluctuations are suppressed close to the wall. Taking the continuity equation into consideration, it is possible to prove that the Reynolds stress must fulfill the following condition [24]:

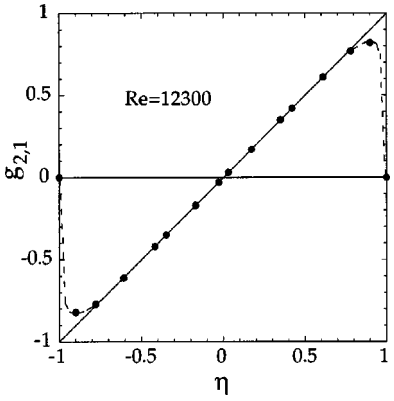

FIG. 7. The Reynolds shear stress at a Reynolds number of 12 300 has already converged very closely to the theoretically proposed profile for the infinite Reynolds number limit. The experimental data (see Refs. [13] or [23]) have been inflected at the origin of the coordinate system to complete the time-averaged turbulent shear stress profile.

$$\lim_{x_2 \to \pm a} \overline{u_2' u_1'} \propto (a \mp x_2)^n, \quad n \geqslant 3. \tag{90}$$

For a generalized solution, based on Prandtl's mixing-length theory, describing the profiles in the viscous sublayer and the boundary layer, it is found that $n=2$. The solution presented in [11], which is derived by applying the DQTM to the plane Couette flow problem, even leads to $n=1$. Because of this failure, one concludes that the related solutions do not yield the correct description for the boundary layer region. But they present very convincing analytical results for the core region. The same reasoning is also valid for the solutions of the plane Poiseuille flow problem presented in this paper.

The drawback of failing to have an overall description of high quality can be easily understood by studying the applied ''mixing lengths'' for the different flow regions (see Fig. 8). In Sec. IV and in Ref. [9] it is explained that—in the context of the DQTM—a mixing length does not have exactly the same meaning and definition as in Prandtl's theories. The solution for the sublayer can be interpreted as being related to a ''mixing length'' that is small compared with the dissipation length. This is compatible with the result that in this first domain the Reynolds stress is negligible. It is well known that in turbulence near walls, in the boundary layer, the mixing length must be proportional to the wall distance. Therefore it is clear that our approach—with a constant mixing length—cannot yield the correct solutions for this domain. Only the third domain, the core region, shows a large constant mixing length, equal to half the distance between the plates. A distribution of the mixing length as proposed above is also reported for Couette flow in the book on turbulence published by Libby (see Ref. [27]), who writes the following: ''There is a temptation to assume that the mixing length is constant throughout the central portion of the flow and varies only within the wall layer.'' Furthermore, he states that ''Briefly, it is not possible to match a solution for the wall layer to that for an outer flow involving a constant mixing length. We thus conclude that at the edges of the outer flow the mixing length must vary as in channel flow, i.e., it must become proportional to the wall distance.'' This

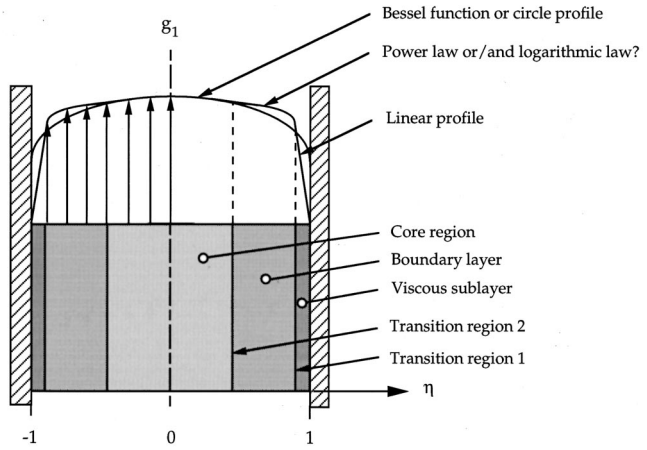

FIG. 8. From the plate toward the center, the plane Poiseuille flow regions are as follows: the viscous sublayer, the boundary layer, and the core region (shaded domains). Between each of these a small transition region occurs. The related functions describing the mean velocity profile are shown above. The three functions add together to give a bulbous velocity profile as occurring in highly turbulent flows. The Bessel functions and the circle profile, which—because of the scaling applied to this graphics—is drawn as an ellipse, guarantee the necessary symmetry requirement $g_1(-\eta)=g_1(\eta)$.

is in agreement with our assumption that in a description of the flow in the boundary layer the model for plane Couette flow in [11] and the theory in this paper have to be modified, by changing the mixing length to be proportional to $(a-x_2)$.

Solving the fluid dynamic equations and simultaneously applying the DQTM yields analytical results for the most important basic turbulent-free shear flow problems. It also analytically describes flow profiles in the core region of plane turbulent Couette and Poiseuille flows very precisely. The infinite Reynolds number solutions of Poiseuille flow are an elevated semicircle, describing the mean velocity profile and a linear function representing the Reynolds shear stress. In accordance, without even applying a closure scheme, a linear function also follows from a dimensional analyses (see Ref. [27]).

Furthermore, in plane Couette and Poiseuille flow—with different symmetries—in both cases an identical order/disorder model of turbulence has been revealed. This is in accordance to many fields, where statistical physics applies to describe the degree of disorder occuring in a system.

X. OUTLOOK

Modifying the DQTM to allow for a space-dependent mixing-length and applying it to the Navier-Stokes equation and solving for the law of the wall will show if this turbulence model is appropriate to also describe turbulent behavior closer to walls. Note that following some papers of Barenblatt and Chorin, e.g., Ref. [28], discussions are indeed performed, if in the boundary layer the mean velocity profiles show a Reynolds-number dependent scaling power law, or are more accurately described by the well established logarithmic law of the wall.

It seems appropriate to refer to the solutions for the boundary layer—derived with the use of the DQTM—in a separate paper. The reason is that the results will be valid for several types of turbulent boundary-layer flows: plane ''wall-turbulent'' flow, plane and axisymmetric Couette and Poiseuille flows, etc. When this problem has been solved, it will be straightforward to also determine the locations of the intersections (δ' and δ'', see Ref. [27]) of the three domains and the function $\alpha(\mathrm{Re})$, relating the shear stress parameter α to the Reynolds number Re. Furthermore, from $\alpha_{\mathrm{crit}}=0.5$ the critical Reynolds number $\mathrm{Re}_{\mathrm{crit}}$ will be obtained.

ACKNOWLEDGMENTS

The authors are grateful to S. Grossmann for enlightening remarks several years ago. We also thank W. Möhring, F. Obermeier, and J. Magnaudet for helpful comments.

[1] N. Gilbert and L. Kleiser, in *Near-wall Turbulence, 1988 Zoran Zorić Memorial Conference*, edited by S. J. Kline and N. H. Afgan (Hemisphere, New York, 1990).
[2] N. D. Sandham, *A Model Equation for Transitional and Turbulent Plane Channel Flow*, edited by F. Durst, B. E. Launder, F. W. Schmidt, and J. H. Whitelaw, selected papers from the Eigth Symposium on Turbulent Shear Flows, Munich, 1993 (Springer-Verlag, Berlin, 1993), pp. 67–80.
[3] S. Grossmann and D. Lohse, Phys. Rev. E **50**, 2784 (1994).
[4] A. Praskovsky and S. Oncley, Phys. Fluids A **6**, 2886 (1994).
[5] M. M. Stanišić, *The Mathematical Theory of Turbulence* (Springer-Verlag, Berlin, 1988).
[6] L. Prandtl, Z. Angew. Math. Mech. **5**, 136 (1925).
[7] J. L. Lumley, J. Appl. Mech. **50**, 1097 (1983).
[8] P. W. Egolf, Helv. Phys. Acta **64**, 944 (1991).
[9] P. W. Egolf, Phys. Rev. E **49**, 1260 (1994).
[10] P. W. Egolf and D. A. Weiss, Phys. Rev. E **58**, 459 (1998).
[11] P. W. Egolf and D. A. Weiss, Phys. Rev. Lett. **75**, 2956 (1995).
[12] C. Itzykson and J.-M. Drouffe, *Statistical Field Theory* (Cambridge University Press, 1992), Vols. 1 and 2.
[13] S. I. Pai, J. Appl. Mech. **20**, 109 (1953).
[14] H. Schlichting, *Boundary-Layer Theory* (McGraw-Hill, New York, 1979).
[15] J. O. Hinze, *Turbulence*, 2nd ed. (McGraw-Hill, New York, 1975).
[16] A. S. Monin and A. M. Yaglom, *Statistical Fluid Mechanics: Mechanics of Turbulence* (MIT Press, Cambridge, 1971).
[17] H. Tennekes and J. L. Lumley, *A First Course in Turbulence* (MIT Press, Cambridge, 1997).
[18] The amplification can be explained by an underlying eddy density model as introduced by Kolmogorov. Our description is still a little vague and shall be further improved.
[19] L. Prandtl, Z. Angew. Math. Mech. **22**, 241 (1942).
[20] In turbulence research the eddy diffusivity is defined in analogy to the diffusivity in kinetic gas theory, where it also is a coefficient of a driving gradient. Analogously one can define a modified eddy diffusivity, by taking the terms into consideration which in the DQTM occur in front of the difference quotient.
[21] S. Corrsin, Adv. Geophys. **18A**, 25 (1974).
[22] *Pocketbook of Mathematical Functions*, edited by M. Abramowitz and I. A. Stegun (Verlag Harri Deutsch, Thun, 1965).
[23] J. Laufer, National Advisory Committee for Aeronautics Technical Report No. 1174, 1954.
[24] H. Reichhardt, Z. Angew. Math. Mech. **31(7)**, 208 (1951).
[25] M. V. Zagarola, A. E. Perry, and A. J. Smits, Phys. Fluids **9**, 2094 (1997).
[26] M. V. Zagarola and A. J. Smits, A new mean velocity scaling for turbulent boundary layers, (Proceedings of the FEDSM'98, ASME Fluids Engineering Division Summer Meeting, June 21–25, Washington DC, 1998).
[27] P. A. Libby, *Introduction to Turbulence* (Taylor & Francis, New York, 1996).
[28] G. I. Barenblatt and A. J. Chorin, ASME Appl. Mech. Rev. **50**, 413 (1997).